Supplementary Information for: Precisely Sculpting Complex Attractor Landscapes through Topological Design

Huayifu Lv[1]

[1]International Academic Center of Complex Systems, Beijing normal university Zhuhai campus, China.

This Supplementary Information contains the mathematical derivations, extended motif constructions, and robustness analyses cited in the main text.

A Conservation, Positivity, and the SP Relation to E–I Descriptions

The labels sharing and plundering describe the signs of the off-diagonal entries. We first decompose the signed weights as $S_{ij} = [w_{ij}]_+$ and $P_{ij} = [-w_{ij}]_+$. The proof then uses only the state-dependent graph matrix

$$\dot{\mathbf{X}} = L(\mathbf{X})\mathbf{X}, \qquad \dot{x}_i = \sum_j L_{ij}(\mathbf{X})x_j, \qquad \mathbf{1}^\mathsf{T} L(\mathbf{X}) = 0.$$

$$L_{ij}(\mathbf{X}) = \begin{cases} w_{ij}, & w_{ij} > 0, \\ w_{ij}, & w_{ij} < 0 \text{ and } x_i > 0, \\ 0, & w_{ij} < 0 \text{ and } x_i = 0, \end{cases} \qquad i \neq j,$$

$$L_{jj}(\mathbf{X}) = -\sum_{i \neq j} L_{ij}(\mathbf{X}).$$

A.1 Conservation

For the resource-conserving SP dynamics defined above, the column-sum condition gives conservation of the total resource inherited from initialization:

$$\frac{d}{dt}\sum_i x_i = \mathbf{1}^\mathsf{T}\dot{\mathbf{X}} = \mathbf{1}^\mathsf{T} L(\mathbf{X})\mathbf{X} = 0.$$

A.2 Nonnegative Invariance

Consider the boundary $x_i = 0$. The boundary flux rule switches off every negative entry in row i, while positive entries remain nonnegative. Since $L_{ii}x_i = 0$ on this boundary,

$$\dot{x}_i\big|_{x_i=0} = \sum_{j \neq i} L_{ij}(\mathbf{X})x_j = \sum_{\substack{j \neq i \\ w_{ij} > 0}} w_{ij}x_j \geq 0.$$

Thus the vector field points inward on every coordinate face, so a nonnegative initial state cannot cross into the negative orthant. Conservation then makes the initial-total simplex $\mathcal{S}_{C_0}$ forward invariant.

A.3 Protected Boundary Transfer and Proportional Splitting

For a node i at the zero-resource boundary, define its sharing income, the nominal demand of plunderer j, and the total nominal plundering demand by

$$r_i(\mathbf{X}) = \sum_{\substack{j \neq i \\ w_{ij} > 0}} S_{ij} x_j, \qquad d_{ij}(\mathbf{X}) = P_{ij} x_j, \qquad D_i(\mathbf{X}) = \sum_{\substack{j \neq i \\ w_{ij} < 0}} d_{ij}(\mathbf{X}).$$

Suppose $x_i = 0$ and $0 < r_i < D_i$. In a protected step of length h, sharing first supplies hr_i units to node i. All plundering channels directed at that victim then act simultaneously for a substep of length $\theta_i h$, where

$$hr_i = \theta_i h D_i, \qquad \theta_i = \frac{r_i}{D_i} \in (0, 1).$$

The transfer from victim i to plunderer j is consequently

$$\Delta Q^{(h)}_{i \to j} = \theta_i h d_{ij} = hr_i \frac{d_{ij}}{D_i}, \qquad \sum_{j:\, w_{ij} < 0} \Delta Q^{(h)}_{i \to j} = hr_i.$$

Thus the node remains at zero resource while its incoming sharing resource is redistributed among its plunderers in the demand proportions d_{ij}/D_i. Repeating the protected step and taking $h \to 0$ defines the corresponding continuous boundary limit, with mean edgewise flow $\bar{f}_{i \to j} = r_i d_{ij}/D_i$.

A.4 Sliding Dynamics and Proportional Splitting at a Zero-Resource Boundary

The construction above describes the local balance on one zero-resource face. The numerical implementation advances the complete network from $\mathbf{X}^k$ in two conservative stages. First, it computes every sharing request from $\mathbf{X}^k$. For each sharing source, its requested outgoing total is capped by its resource at the start of the step; all resulting sharing transfers are then applied together, giving the intermediate state $\widetilde{\mathbf{X}}^{k+1}$. Second, for every potential victim i, the available stock is $\widetilde{x}_i^{k+1}$. The active plunderers are the nodes j with $P_{ji} > 0$ and $x_j^k > 10^{-12}$. Their total draw is capped before the update,

$$q_i^k = \min\left\{ h \sum_j P_{ji} x_j^k,\ \widetilde{x}_i^{k+1} \right\},$$

and this finite amount is distributed among them in the demand proportions $P_{ji} x_j^k$. The plundering increments for all victims are accumulated and then applied together. Thus sharing cannot overdraft its source at the first stage, and plundering cannot overdraft its victim at the second stage: the update selects a legal outflow before applying it, rather than computing a negative state and clipping it afterwards. A node that is zero at $\mathbf{X}^k$ but receives sharing during the first stage becomes eligible to plunder on the next step, because plunderer eligibility is evaluated from $\mathbf{X}^k$. Every realized transfer is subtracted from one node and added to another by the same amount, so total resource is conserved. The final nonnegative clamp only removes round-off-scale near-zero values; it can introduce at most a machine-precision-scale total-resource error and does not alter the conservation dynamics or the qualitative numerical outcomes reported here.

A.5 Structural Coupling of Interaction and Self Terms in SP and E–I Equations

For comparison, a standard local linear form of an E–I rate model can be written as [1]

$$\tau \dot{\mathbf{r}} = -\Lambda \mathbf{r} + E\mathbf{r} - I\mathbf{r} + \mathbf{u}, \qquad E_{ij} \geq 0, \quad I_{ij} \geq 0.$$

Here $\mathbf{r}$ denotes the conventional state vector, E and I specify positive and negative recurrent cross-coordinate contributions, Λ is an independently specified diagonal self term, conventionally chosen as leak or self-relaxation, and $\mathbf{u}$ is external drive. These ingredients can be changed separately: modifying a recurrent edge does not require a corresponding change of a diagonal coefficient.

SP differs at exactly this point: its diagonal self terms are structurally tied to the same signed topology that specifies the off-diagonal interactions. To expose this matrix structure, first consider the all-positive interior of the SP dynamics, where every prescribed plundering edge is effective. With

$$D_S = \mathrm{diag}(S^{\mathsf{T}}\mathbf{1}), \qquad D_P = \mathrm{diag}(P^{\mathsf{T}}\mathbf{1}),$$

$$\dot{\mathbf{X}} = \underbrace{S\mathbf{X}}_{\text{sharing inflow}} - \underbrace{D_S\mathbf{X}}_{\text{structured sharing leakage}} - \underbrace{P\mathbf{X}}_{\text{plundering victim loss}} + \underbrace{D_P\mathbf{X}}_{\text{structured plundering self-gain}}.$$

The off-diagonal term $S_{ij}x_j$ has the same sign as a positive recurrent contribution $E_{ij}r_j$. One sharing edge indexed by (i,j) inserts $+S_{ij}x_j$ into $\dot{x}_i$ and $-S_{ij}x_j$ into $\dot{x}_j$. Summing the latter contributions over all targets gives $-(D_S)_{jj}x_j$, where $(D_S)_{jj} = \sum_i S_{ij}$. The sharing block therefore contains a negative diagonal self term, algebraically comparable to self-relaxation, whose coefficient is fixed by the outgoing sharing column of S; it is not an independently chosen leak.

The off-diagonal term $-P_{ij}x_j$ has the same sign as a negative recurrent contribution $-I_{ij}r_j$. For the same indexed edge, column balance inserts $+P_{ij}x_j$ into $\dot{x}_j$. Summing over all targets yields $+(D_P)_{jj}x_j$, with $(D_P)_{jj} = \sum_i P_{ij}$. The plundering block therefore contains a positive diagonal self term, algebraically comparable to self-excitation, whose coefficient is fixed by the same outgoing column of P that generates the negative cross-coordinate terms; it is not an independent self-loop parameter.

Combining the four SP terms makes the E–I correspondence explicit: S plays the role of E, P plays the role of I, and the complete SP diagonal $D_P - D_S$ occupies the algebraic position of $-\Lambda$. Equivalently, $\Lambda_{\mathrm{SP}} = D_S - D_P$. Unlike the independently prescribed Λ in the standard form, Λ_{SP} may contain both self-relaxing and self-amplifying coordinates, and every coefficient is fixed by the sharing and plundering edges incident from that source column.

$$\mathbf{1}^{\mathsf{T}}(S - D_S) = 0, \qquad \mathbf{1}^{\mathsf{T}}(D_P - P) = 0.$$

This strict tying of interaction terms to diagonal self terms is the central algebraic difference between SP and a standard E–I equation with independently adjustable recurrent, diagonal, and drive parameters. The signed graph fixes both the signs and zero pattern of cross-coordinate terms and the diagonal completions that make the sharing and plundering blocks column-balanced. Hence $\mathbf{1}^{\mathsf{T}}L = 0$: the SP equation as defined contains no counterpart of the external drive $\mathbf{u}$, and its total state has no net source or sink. A source or sink can be added only as a separate non-conservative extension that changes total resource.

The preceding decomposition applies only while every victim coordinate is positive. When the boundary rule is active, the full nonlinear equation replaces P, its diagonal completion D_P, and hence $\Lambda_{\mathrm{SP}} = D_S - D_P$, simultaneously by

$$P_{ij}(\mathbf{X}) = \begin{cases} P_{ij}, & x_i > 0, \\ 0, & x_i = 0, \end{cases} \qquad (i \neq j), \qquad D_P(\mathbf{X}) = \mathrm{diag}\big(P(\mathbf{X})^{\mathsf{T}}\mathbf{1}\big),$$

$$L(\mathbf{X}) = S - D_S + D_P(\mathbf{X}) - P(\mathbf{X}).$$

When $x_i = 0$, every entry $P_{ij}(\mathbf{X})$ in victim row i is set to zero. By the definition of $D_P(\mathbf{X})$, the corresponding j-th column sum then removes the same P_{ij} term, so the associated coefficient in $\Lambda_{\mathrm{SP}}(\mathbf{X}) = D_S - D_P(\mathbf{X})$ changes as well. The nonlinear boundary condition therefore preserves the same structural tying: a negative plundering interaction, its positive diagonal self term, and the complete effective diagonal all switch together. Effective-graph switching is thus a state-dependent change of coupled matrix coefficients, not a scalar clipping operation applied after an otherwise fixed linear system. Because this matrix update itself keeps the state in the nonnegative conserved domain, no additional activation, saturation, or global-normalization function is required to limit the state range.

B Global Convergence of an Isolated Citadel

B.1 Pure-Sharing Linear System

We first state the graph-theoretic condition used throughout this appendix. For a pure-sharing citadel, let $S = [W]_+$ and define its directed sharing support as $G_S = (V, E_S)$, with $j \to i \in E_S$ exactly when $S_{ij} = w_{ij} > 0$. The support is *strongly connected* when, for every ordered pair of nodes $u, v \in V$, there is a finite directed path from u to v using edges in E_S. Direct reciprocal edges, symmetry, and all-to-all connectivity are not required. In the present matrix convention, this is equivalent to the nonnegative matrix S being irreducible: for every source j and target i, there exists an integer $m \geq 0$ for which $(S^m)_{ij} > 0$. Since the off-diagonal support of the pure-sharing generator L is exactly that of S, the same condition says that L is an irreducible Metzler matrix.

Let the citadel contain n nodes. For $i \neq j$, let $w_{ij} > 0$ when the sharing edge $j \to i$ is present and let $w_{ij} = 0$ otherwise. Assume that this directed support graph is strongly connected. With no plundering edge and no external source or sink, the effective matrix is independent of the state:

$$L_{ij} = w_{ij} \quad (i \neq j), \qquad L_{jj} = -\sum_{i \neq j} w_{ij} = -r_j, \qquad \dot{\mathbf{X}} = L\mathbf{X}.$$

$$\mathbf{1}^\top L = 0, \qquad \mathbf{X}(t) = e^{Lt}\mathbf{X}(0).$$

The matrix L is therefore an irreducible Metzler matrix with zero column sums. Appendix A already implies that the simplex $\mathcal{S}_{C_0}$ is forward invariant. What remains is to show that its flow has exactly one fixed profile.

B.2 Convergence Theorem

Theorem B.1. For any fixed strongly connected sharing support and any choice of strictly positive weights on its edges, there exists a unique vector $\boldsymbol{\pi} > 0$ such that

$$L\boldsymbol{\pi} = 0, \qquad \mathbf{1}^\top \boldsymbol{\pi} = 1.$$

For every $\mathbf{X}(0) \geq 0$ with $C_0 = \mathbf{1}^\top \mathbf{X}(0)$, the solution satisfies

$$\lim_{t\to\infty} \mathbf{X}(t) = \lim_{t\to\infty} e^{Lt}\mathbf{X}(0) = C_0\boldsymbol{\pi}.$$

Hence the intersection of the fixed-point set with $\mathcal{S}_{C_0}$ is the singleton $\{C_0\boldsymbol{\pi}\}$, and its basin is the entire simplex. Strong connectivity determines that the isolated citadel has one globally attracting fixed profile. The particular edge weights determine that profile, as well as the trajectory and rate by which resources approach it.

B.3 Proof by Uniformization and Perron–Frobenius Theory

Proof. Choose $\alpha > \max_j r_j$ and define the auxiliary matrix

$$Q = I + \frac{1}{\alpha}L.$$

Every entry of Q is nonnegative, every diagonal entry is strictly positive, and $\mathbf{1}^\top Q = \mathbf{1}^\top$. Thus Q is a column-stochastic matrix. Its directed support contains the strongly connected sharing graph and a self-loop at every node, so Q is primitive. The Perron–Frobenius theorem gives a unique normalized vector $\boldsymbol{\pi} > 0$ with $Q\boldsymbol{\pi} = \boldsymbol{\pi}$, and

$$\lim_{k\to\infty} Q^k = \boldsymbol{\pi}\mathbf{1}^\top.$$

Because $L = \alpha(Q - I)$, the continuous-time semigroup has the uniformization expansion

$$e^{Lt} = e^{-\alpha t}e^{\alpha t Q} = e^{-\alpha t}\sum_{k=0}^{\infty} \frac{(\alpha t)^k}{k!} Q^k.$$

The coefficients $e^{-\alpha t}(\alpha t)^k/k!$ sum to one and form a Poisson distribution with mean αt. This does not introduce stochasticity into the SP dynamics: it is an exact algebraic representation of e^{Lt} as a weighted average of Q^k. As $t \to \infty$, the weight assigned to every fixed finite range of k vanishes, while $Q^k \to \boldsymbol{\pi}\mathbf{1}^\top$ at large k. Therefore

$$\lim_{t\to\infty} e^{Lt} = \boldsymbol{\pi}\mathbf{1}^\mathsf{T}, \qquad \lim_{t\to\infty} \mathbf{X}(t) = \boldsymbol{\pi}\mathbf{1}^\mathsf{T}\mathbf{X}(0) = C_0\boldsymbol{\pi}.$$

The Perron eigenvalue of Q is simple and all its other eigenvalues have modulus strictly below one. Equivalently, zero is a simple eigenvalue of L, while every other eigenvalue has strictly negative real part. This completes the proof.

B.4 Scope of the Weight-Robust Statement

The theorem imposes no equality, symmetry, or narrow numerical interval on the sharing weights. The qualitative result holds throughout the full positive orthant associated with a fixed strongly connected support: changing the weights continuously changes the normalized profile $\boldsymbol{\pi}$ and the convergence speed, but it cannot create a second fixed profile or destroy convergence. The statement ceases to be guaranteed only when an edge weight reaches zero in a way that destroys strong connectivity, because that operation changes the support topology itself.

C Three-Node Limit Cycles: Interior Spectrum and Boundary Restart

Directed cyclic inhibition is a topological intuition for sequential activity or oscillation in network dynamics: directed negative feedback biases phase-shifted switching, but does not itself guarantee sustained oscillation. The three-node SP circulation asks how this intuition is realized under resource conservation and zero-resource boundary switching. When every component of the state vector is strictly positive, the system lies in a linear interior region whose effective matrix has an explicit dynamical spectrum: the imaginary part of a conjugate pair gives a rotating component, while the real part determines decay, neutrality, or growth. Once a coordinate reaches zero, the boundary rule changes the subsequent dynamics, so the spectrum alone does not determine whether the global outcome is a periodic orbit or a boundary lock. This appendix therefore follows the hierarchy from cyclic topology to interior spectrum, from spectrum to rotating modes, and from rotating modes to possible global attractor regimes. Sections C.1–C.4 develop this hierarchy. Figure C2 then shows directly that sustained circulation survives substantial independent perturbations of microscopic edge magnitudes. Motivated by this broad numerical robustness, Section C.5 reverses the usual parameter-search question: instead of asking where the construction first begins to work, it fixes the sharing ring and deliberately searches for a directed plundering imbalance that makes it fail.

We begin with the equal-edge baseline: all three sharing edges carry the same weight $s > 0$, and all three plundering edges carry the same weight $-p < 0$. This symmetric three-node ring is the analytic starting point. After establishing its interior spectrum and boundary regimes, we relax the equal-weight condition and test whether the same organization persists under independently heterogeneous edge weights.

C.1 Exact Spectrum of the Positive Three-Node Interior

Let sharing and plundering resource flows follow the same cyclic order $1 \to 2 \to 3 \to 1$. Write the sharing weight as $s > 0$ and the plundering edge weight as $-p < 0$, where $p > 0$. While $x_1, x_2, x_3 > 0$, no boundary channel has yet been disabled and the state-dependent dynamics reduces exactly to the linear system

$$\dot{\mathbf{x}} = \begin{pmatrix} p-s & -p & s \\ s & p-s & -p \\ -p & s & p-s \end{pmatrix} \mathbf{x}, \qquad \dot{x}_i = s x_{i-1} + (p-s)x_i - p x_{i+1},$$

with cyclic indices. For $\omega_k = e^{2\pi i k/3}$, the Fourier vectors $v^{(k)} = (1, \omega_k, \omega_k^2)^\mathsf{T}$ diagonalize the matrix. The corresponding eigenvalues are

$$\lambda_0 = 0, \qquad \lambda_\pm = \frac{3}{2}(p-s) \pm i\frac{\sqrt{3}}{2}(p+s).$$

The zero eigenvalue is the conserved total-resource mode. The conjugate pair acts in the two-dimensional plane $\sum_i x_i = C$: its real part controls damping or amplification, while its imaginary part produces cyclic rotation. Before the first boundary contact, each component can therefore be written as

$$x_j(t) = \frac{C}{3} + Re^{\alpha t}\cos\left(\omega t - \frac{2\pi(j-1)}{3} + \phi\right), \qquad \alpha = \frac{3}{2}(p-s), \quad \omega = \frac{\sqrt{3}}{2}(p+s).$$

Here $C = \sum_i x_i$ is fixed, and R and ϕ are selected by the microscopic initial allocation. This formula is exact only until the first coordinate reaches zero. It therefore identifies the interior mechanism that creates rotation, but it does not by itself determine the global attractor of the nonnegative system. Figure C1(A) plots this interior prediction beside the dynamics under the boundary rule.

C.2 Three Spectral Regimes

Figure C1(A) shows the three consequences of the sign of α. If $s > p$, then $\alpha < 0$: every nonuniform component undergoes damped oscillation and the state converges to the uniform fixed profile $(C/3, C/3, C/3)$. If $s = p$, then $\alpha = 0$: on the conserved plane $x_1 + x_2 + x_3 = C$, the positive-interior linear flow is an exact Euclidean rotation about $(C/3, C/3, C/3)$. Every noncentral orbit is therefore a circle centered at the uniform profile. The conservation simplex is an equilateral triangle: circles of radius below its inradius $C/\sqrt{6}$ lie wholly inside it and form a neutrally stable continuum of closed trajectories, rather than attracting interior limit cycles. Along the initial-state ray $x^{(q)}(0) = (1-q)(C/3, C/3, C/3) + q(C, 0, 0)$, the circle radius is $qC\sqrt{2/3}$; hence the first orbit to graze a simplex face occurs exactly at $q = 1/2$, at $(2C/3, C/6, C/6)$. For $q > 1/2$, the unconstrained circle would cross the triangle boundary. The protected SP dynamics instead changes its effective flow at contact; numerically, all tested $q \geq 1/2$ converge to the same boundary-touching periodic orbit, whereas $q < 1/2$ retains its distinct interior circle. If $s < p$, then $\alpha > 0$: the rotating nonuniform mode grows until a coordinate reaches zero.

The right-hand panel of Figure C1(A) shows how the boundary rule turns the growing interior rotation into a periodic trajectory. When $s < p$, the interior linear equation first amplifies the rotating nonuniform component until one node reaches zero. At that contact, the node's outgoing plundering is switched off; sharing then returns a positive seed to the depleted node and the resource flow starts around the ring again. This sequence—boundary contact, channel closure, and restart—keeps the trajectory within the bounded nonnegative conservation simplex and, when the restart path and parameter regime are appropriate, supports a periodic orbit. If the nonnegative boundary is removed, the linear solution simply crosses zero and its positive and negative amplitudes keep growing.

C.3 Pure Cyclic Plundering Rotates but Cannot Restart

Setting $s = 0$ gives $\lambda_\pm = 3p/2 \pm i\sqrt{3}p/2$. Thus, even without sharing, cyclic plundering produces and amplifies a rotating component while all nodes remain positive. Figure C1(B) shows why this is still insufficient for sustained circulation. Continuing the same linear equation through zero produces unbounded positive and negative components. Under the nonnegativity rule, by contrast, the first depleted node loses its outgoing plundering channel. Because pure cyclic plundering provides no route that can reseed that node, the trajectory reaches a boundary lock instead of restarting the cycle.

At a single-node state such as $(C, 0, 0)$, the next plundering port has no resource and therefore cannot activate its outgoing plundering relation. Because a pure plundering ring contains no edge that can place a positive seed on that port, the state is absorbing under the boundary rule. The example in Figure C1(B) locks at node 2; cyclic permutations give the other two possible locks. Thus, even when the spectrum of the interior linear region indicates a rotating mode, nonlinear, state-dependent boundary switching can still lock the trajectory onto the zero-resource face. This example therefore shows why the spectral analysis of the interior matrix is only a guide: the full system is state-dependent and nonlinear, so each boundary contact changes the effective matrix. It cannot by itself serve as a strict predictor of the global dynamics.

C.4 Conservative Restart Is Not Unique to a Sharing Ring

A one-way plundering edge is active only while its plundering end holds resource. Figure C1(B) exposes the resulting dynamical tension: a node at exactly zero cannot plunder its target, yet an arbitrarily small positive seed immediately reopens its outgoing plundering channel and is amplified by the ensuing unilateral transfer. Restart becomes possible when the node that previously plundered and suppressed it has itself reached zero, so that the new seed is no longer removed. The seeded node can then grow from a small amount of resource. Sustained circulation therefore requires only a pathway that supplies a small amount of startup resource to a depleted port at the appropriate time. A co-directed sharing ring, a central neutralizer, and port-specific reserve nodes provide three topologically different ways to do so.

Panels C1–C3 of Figure C1 realize this condition in three topologically different ways. C1 places the restart path directly on the outer ring: the occupied predecessor shares a seed with the depleted successor. This is the construction used for the principal three-node cycle in the main text. C2 places a neutral center that shares symmetrically with all three circulation ports. In the displayed symmetric construction, this center remains at their mean resource level, so it can supply a depleted port with resource and restart the cycle. C3 gives each plundering port its own reserve node. The reserve node has no plundering link to or from the circulation network and is connected only by constant-strength sharing. While its paired circulation port is held at zero, resource leaves the reserve through this sharing edge, so the amount remaining in the reserve decays exponentially rather than disappearing instantaneously. The reserve can therefore remain positive until the direct downstream node that plunders and suppresses the paired port is itself cleared. Its suppressive channel then becomes ineffective; resource still held by the reserve flows through the sharing edge into the paired port, moves it away from the boundary, and restarts the circulation. During the subsequent rising phase of that port, the same sharing connection replenishes the reserve for the next cycle. In C3, both the initial bars and the resource trajectories display all six nodes $(1, R_1, 2, R_2, 3, R_3)$, whereas the three-dimensional orbit retains only the three circulation nodes (x_1, x_2, x_3). The reserve trajectories therefore make the conservative restart paths explicit, while the three circulation coordinates still reach zero in turn. Together, the three constructions show that the required functional condition is startup resource reaching a depleted port at the appropriate time, and that this condition can be implemented by different sharing architectures.

C.5 From Broad Robustness to an Extreme Failure Boundary

Figure C2A shows that all three restart constructions retain sustained circulation when the signed topology is held fixed and the microscopic edge magnitudes are perturbed independently. In many dynamical models, the practical challenge is to find a parameter window that realizes the desired behavior. Here, ordinary sign-preserving perturbations do not readily destroy the cycle; a clear failure regime appears only under extreme parameter conditions. Figure C2B therefore follows one plundering edge as it is weakened nearly to absence and directly identifies the resulting boundary-capture condition.

Panel A supplies the robustness evidence: the period, waveform, and orbit geometry change, but each restart architecture remains cyclic. Panel B then holds $s = 0.020$, $p_1 = p_2 = 0.100$, $C = 100$, and the initial state $(44, 34, 22)$ fixed, while reducing only the third plundering magnitude $p_3 = \rho$ from its symmetric value to a missing edge.

$$\mathbf{p}(\rho) = (0.100,\ 0.100,\ \rho), \qquad 0 \le \rho \le 0.100.$$

The relevant failure face is $x_1 = 0$. While node 2 can remove every sharing seed delivered from node 3 to node 1, that face remains closed. On this face the protected dynamics has the fixed profile

$$(x_1, x_2, x_3) = \left(0,\ \frac{C(1-\rho/s)}{2-\rho/s},\ \frac{C}{2-\rho/s}\right), \qquad 0 \le \rho \le s.$$

$$p_2 x_2 \ge s x_3 \quad \Longleftrightarrow \quad \rho \le p_3^* = s\left(1 - \frac{s}{p_2}\right) = 0.016.$$

The first line gives the resource allocation on the captured face; the second is the self-consistency condition that node 2 can drain every restart seed at node 1. Thus p_3^* is an explicit boundary-capture threshold for this one-edge path. Above it, the displayed initial state continues to circulate; below it, the same state is captured by the face. On the captured face, p_1 is inactive because node 1 has no resource, p_2 maintains the capture condition, and the ratio of the surviving resources is set by p_3/s, namely $x_2/x_3 = 1 - p_3/s$. At $\rho = 0$, the third plundering edge is absent and the profile becomes $(0, 50, 50)$. The missing-edge endpoint therefore provides a definite failure configuration for the direct-sharing double ring.

For the sign-preserving perturbations examined here, the conclusion is direct: sustained circulation occupies a broad working region, whereas failure occupies a very narrow region reached only when a critical plundering edge is weakened to its capture threshold or nearly removed. Ordinary independent magnitude perturbations, including visibly heterogeneous realizations, do not destroy the cycle. The displayed one-edge path therefore gives an explicit captured boundary profile and a sharp observed transition.

C.6 Beyond Three-Node Circulation: Multi-Wave and Alternating-Support Attractors

Figure SC3 asks what new attractor organizations appear when the directed three-node circulation is extended to larger rings. Every row uses the same local co-directed sharing/plundering rule, with sharing weight $s = 0.020$, plundering magnitude $p = 0.100$, and total resource $C = 100$. Sharing remains the restart path. The only construction step is to continue this same directed local rule around a longer ring; the simulations then reveal which additional fixed and periodic resource organizations become available.

The alternating supports of even rings follow directly from parity. For $n = 2m$, the ring has two alternating independent sets, $S_{\text{odd}} = \{1, 3, \ldots, 2m-1\}$ and $S_{\text{even}} = \{2, 4, \ldots, 2m\}$. Consider S_{odd} as the active set. Each intervening even node receives a sharing seed from its active predecessor; once it becomes positive, however, its active downstream neighbor plunders it. In the displayed $p > s$ regime, this clearing prevents the seed from accumulating into an independently sustained support, so the intervening nodes remain in a near-zero boundary layer while the alternating support persists. No two active nodes are nearest neighbors. An odd ring cannot close this alternating assignment: after stepping around the ring, the final and first nodes would have to be both active or both inactive. It therefore has no full alternating support of this type. The two even-ring supports are exchanged by a one-node cyclic shift.

The extension is already qualitatively richer than a mere rescaling of the three-node cycle. Even rings admit alternating non-neighbor fixed supports, whereas odd rings do not admit a full alternating bipartition around the cycle. Larger odd and even rings also permit distinct recurrent organizations, including the five-node mixed wave and the six-node double wave. Figure SC3 therefore records an attractor repertoire generated by one unchanged local signed rule; a complete basin partition or a general classification for arbitrary ring size is a separate question.

D Far-Plundering Topologies and Sign-Robust Support Geometry

D.1 Support Geometry Read Directly from the Plundering Topology

Consider an isolated pure-plundering network with $w_{ij} \leq 0$ for $i \neq j$. To read its support geometry, temporarily forget the magnitudes and directional asymmetry of the negative weights and retain only a relation on unordered node pairs. In the minimal construction, each pair has either no edge in either direction, $w_{ij} = w_{ji} = 0$, or reciprocal plundering, $w_{ij} < 0$ and $w_{ji} < 0$; the two negative magnitudes need not be equal. We therefore define the two pair sets

$$E_P(W) = \big\{\{i,j\} : w_{ij} < 0,\ w_{ji} < 0\big\}, \qquad E_0(W) = \big\{\{i,j\} : w_{ij} = w_{ji} = 0\big\}.$$

Thus $E_P(W)$ is the set of unordered node pairs joined by reciprocal plundering, whereas $E_0(W)$ is the complementary set of pairs with no plundering edge in either direction. The support geometry below is read from the zero-edge relation $E_0(W)$.

Any set of nodes with no plundering edge among its members can retain resource jointly. If $Q \subseteq V$ is such a set, its fixed-total allocations form the face $\Delta_Q(C_0) = \{\mathbf{X} \geq 0 : \operatorname{supp}(\mathbf{X}) \subseteq Q,\ \mathbf{1}^{\mathsf{T}}\mathbf{X} = C_0\}$. No plundering flow is active on this face, so every point of $\Delta_Q(C_0)$ is fixed. These fixed faces, together with their boundary faces, form the support complex determined by the zero pattern of the plundering topology.

D.2 Spectral Boundary Lemma

Consider any connected component H of the currently positive reciprocal-plundering graph, and let L_H denote its pure-plundering matrix: its off-diagonal entries are the negative plundering terms and its diagonal entries are fixed by the zero-column-sum rule. Before a boundary is reached, $\dot{\mathbf{X}}_H = L_H\mathbf{X}_H$. This matrix is the sign-reversed counterpart of the pure-sharing generator in Appendix B. It therefore has one zero eigenvalue, while all nonzero eigenvalues have positive real part. The conserved interior profile is consequently a repelling equilibrium on the fixed-total simplex rather than an attractor.

$$\dot{\mathbf{X}}_H = L_H\mathbf{X}_H, \qquad \operatorname{Re}\lambda(L_H) > 0 \quad (\lambda \neq 0).$$

Unless the initial state lies exactly at the interior stationary profile, a trajectory cannot remain in the interior of a support containing a plundering pair: a coordinate reaches the zero boundary. The exact profile is not an attractor to be included in the terminal geometry. On the fixed-total simplex, every perturbation away from it lies in a mode with positive real part, so its stable set is the profile itself; any arbitrarily small mismatch in the initial allocation drives the trajectory away. Pure plundering supplies no restart mechanism, so the positive support can only shrink. Repeating the argument on the remaining support gives, after finitely many boundary events, a support with no internal plundering pair; all actual plundering fluxes then vanish. Hence the possible terminal supports are precisely the node sets with no plundering edge among their surviving members, including states in which only a subset of a larger coexisting set retains resource.

D.3 Universal Construction of Line-Complex Attractors

Let $G = (V, E_G)$ be a finite simple triangle-free graph without isolated vertices: for every vertex, no two vertices adjacent to it are adjacent to one another. We show that G can be directly realized as the graph topology of a continuous-attractor support. Put zero plundering weights exactly on the edges of G and reciprocal plundering on every other pair. By D.2, the terminal support complex is the clique complex of G. Since G is triangle-free and has no isolated vertices, every maximal clique contains exactly two vertices—a 2-clique, or equivalently an edge of G. Its maximal attractor faces are therefore precisely one-dimensional resource segments. Denote the resulting fixed-total attractor set at total resource C_0 by $\mathcal{A}_{C_0}(G)$; it is the union of these segments:

$$w_{ij} = w_{ji} = 0 \iff \{i,j\} \in E_G, \qquad w_{ij} < 0,\ w_{ji} < 0 \iff \{i,j\} \notin E_G,$$

$$\mathcal{A}_{C_0}(G) = \bigcup_{\{i,j\}\in E_G} \Delta_{\{i,j\}}(C_0).$$

This is a topology compiler for graph-structured continuous attractors: several zero-plundering edges meeting at one node give a junction or branch, while a closed sequence of zero-plundering edges gives a closed continuous route. The claim is only about incidence—which support segments meet and which continuous routes exist. Metric geometry and any additional transport interpretation must be introduced separately.

D.4 Ring Family and Sign-Preserving Weight Changes

For an n-node far-plundering ring, arrange the nodes cyclically, leave every nearest-neighbor pair unlinked, and place reciprocal plundering between every non-neighbor pair. The largest node sets with no plundering edge among them are exactly the adjacent pairs. Their fixed-total line segments meet at the pure-node states and form a closed one-dimensional support complex:

$$\mathcal{A}_{C_0} = \bigcup_{i=1}^{n} \Delta_{\{i,i^+\}}(C_0), \qquad i^+ = 1 + (i \bmod n).$$

Figure D1 illustrates this result for six-, seven-, and eight-node rings and for two negative-weight assignments of the six-node case. Changing negative magnitudes can alter boundary order, basin boundaries, terminal allocation, or the allowed face selected by a given start; it cannot change the family of adjacent-pair and singleton supports while the zero pattern and negative-edge support are fixed.

The robustness domain is the whole open negative orthant associated with one fixed zero pattern. Reciprocal directions and different edges need not have equal magnitudes; node degree requires no compensating weight ratio. Only a zero-pattern or sign change alters the support complex.

A related six-unit threshold-linear construction obtains the corresponding ring by parameter tuning [2]. On the corresponding active support, its reduced linear equation agrees with the present six-node far-plundering construction. Both descriptions recognize the same geometric fact: line-attractor segments joined end to end can form a one-dimensional ring attractor.

D.5 Unequal Topological Status: a T-Junction Support Complex

Although the related six-unit threshold-linear ring construction obtains the same reduced ring dynamics, it remains tied to a rotationally symmetric node arrangement and to precisely selected parameter values. It therefore does not provide a topology-first construction rule for continuous attractors with unequal node roles or branching support geometry. The far-plundering rule does: it requires only that intended coexistence pairs carry zero reciprocal plundering and all other pairs carry reciprocal plundering.

The construction does not require nodes to occupy equivalent topological positions. In the seven-node system of Figure D2, the six unlinked pairs $\{1,2\}$, $\{1,3\}$, $\{1,4\}$, $\{2,5\}$, $\{3,6\}$, and $\{4,7\}$ are the maximal supports. They join into three two-segment arms.

$$\mathcal{K}_{\max}(W_{\mathrm{T}}) = \big\{\{1,2\},\{1,3\},\{1,4\},\{2,5\},\{3,6\},\{4,7\}\big\}.$$

Figure D2 projects the stable terminal-state manifold in the seven-dimensional fixed-total state space onto its first three principal components, making all six coexistence segments visible at once. Representative initial states reach every branch. The nodes have different graph-theoretic roles and degrees, but the construction requires only that the prescribed zero/negative weight signs be retained.

The same construction can encode a T-junction, a crossroads, or an entire street graph at a chosen sampling resolution. Each intended street segment is represented by a chain of zero-plundering pairs, while all nonadjacent sampled nodes reciprocally plunder.

E Sparse Citadel Competition and Internal Sharing

This appendix keeps one paired sparse plundering interface, $X_1 \leftrightarrow Y_1$ and $X_2 \leftrightarrow Y_2$, while changing only the bidirectional sharing magnitude s inside the two citadels. Figure E1 gives the original trajectory-level comparison at zero, weak, and strong sharing. Figure E2 then samples the full four-node conservation simplex and measures how the non-WTA basin contracts along the same sweep. Together, the two figures distinguish representative attractor portraits from a basin-volume statement about this fixed topology.

E.1 Representative Attractor Portraits at Three Sharing Strengths

Figure E1 holds the two reciprocal plundering pairs fixed and repeats the same four initial resource profiles at three internal sharing magnitudes. With no internal sharing, the two local WTA pairs choose independently, yielding pure X, pure Y, and two mixed terminal supports. A weak positive sharing link transmits a local gain or loss from one member to the other: the two pairs are no longer independent, yet mixed outcomes remain because common fate is not enforced. Strong bidirectional sharing within X and within Y finally makes the members of each citadel share a common fate, so the same four starts collapse pairwise onto only the pure X or pure Y outcomes. Internal sharing therefore continuously changes the organization from independent choices, through partially coordinated choices, to two coherent citadels. Figure E2 quantifies this interpolation by scanning the associated basin volumes.

E.2 Basin Contraction under Internal Sharing

With total resource C, the four-node initial state lies in the three-simplex $\Delta^3 = \{x_i \geq 0, \sum_i x_i = C\}$. Each uniformly sampled state is evolved under the same conservative boundary-transfer update and classified by its terminal support: pure X if both Y nodes are zero, pure Y if both X nodes are zero, and non-WTA otherwise. At $s = 0$, pure X, pure Y, and mixed supports all occupy finite regions of Δ^3. As s increases, a local resource gain or loss at one port is transmitted to the other member of the same citadel; the non-WTA basin contracts continuously. For the fixed construction in Figure E2 with $p = 0.035$, the sampled generic initial states reach only pure X or pure Y at $s = p$. Figure E2 reports the resulting basin-volume scan over all of Δ^3.

F Higher-Order Motifs Select a Representation Layer

This appendix records two constructive examples in which a higher-order representation is itself an SP motif. They show a design possibility rather than a general theory of computation. In both examples, the higher-order nodes are ordinary resource-carrying nodes in the same closed graph: no auxiliary readout equation, external classifier, or separate decision mechanism is introduced.

F.1 XOR as a Hierarchy of WTA and Conjunction Motifs

Figure SF1A uses a ten-node topology implementing the XOR relation, with sharing magnitude $s = 0.05$ and plundering magnitude $p = 0.10$. Nodes $1, 2$ and $3, 4$ form two reciprocal-plundering input pairs. Nodes $5, 6, 7, 8$ form a mutually plundering conjunction layer, each receiving reciprocal sharing from one specified member of each input pair: $5 = (1, 3)$, $6 = (1, 4)$, $7 = (2, 3)$, and $8 = (2, 4)$. Nodes 9 and 10 are another reciprocal-plundering pair. Node 9 shares with the two equal conjunctions $5, 8$, while node 10 shares with the two unequal conjunctions $6, 7$. Thus the output layer represents the equality/XNOR versus inequality/XOR organization of the two selected input supports.

The four trajectories in Figure SF1A start from the four different input-pair combinations. They converge respectively to $1 + 3 + 5 + 9$, $1 + 4 + 6 + 10$, $2 + 3 + 7 + 10$, and $2 + 4 + 8 + 9$. A higher-order output node therefore selects a class of conjunction motifs and, through the same graph dynamics, organizes the corresponding lower-level representation layer as a whole. The construction is explicit: the four conjunction supports and the two output classes can be read directly from the signed topology.

F.2 Overlapping Conjunction Supports

Figure SF1B gives a second example in the six-node impossible-triangle motif. The elementary nodes A, B, C are joined by three higher-order conjunction nodes AB, AC, BC. Each conjunction node shares with the two elementary nodes named by its label; the conjunction nodes mutually plunder; and each conjunction node reciprocally plunders the elementary node excluded from its label. The three initial conditions show that the selected conjunction remains with its compatible pair of elementary components while the excluded component is cleared. Hence a higher-order representation can select a compatible distributed support rather than merely activate an isolated output node.

References

[1] Wilson, H. R. & Cowan, J. D. Excitatory and inhibitory interactions in localized populations of model neurons. *Biophysical Journal* **12**, 1–24 (1972).

[2] Noorman, M., Hulse, B. K., Jayaraman, V., Romani, S. & Hermundstad, A. M. Maintaining and updating accurate internal representations of continuous variables with a handful of neurons. *Nature Neuroscience* **27** (2024).

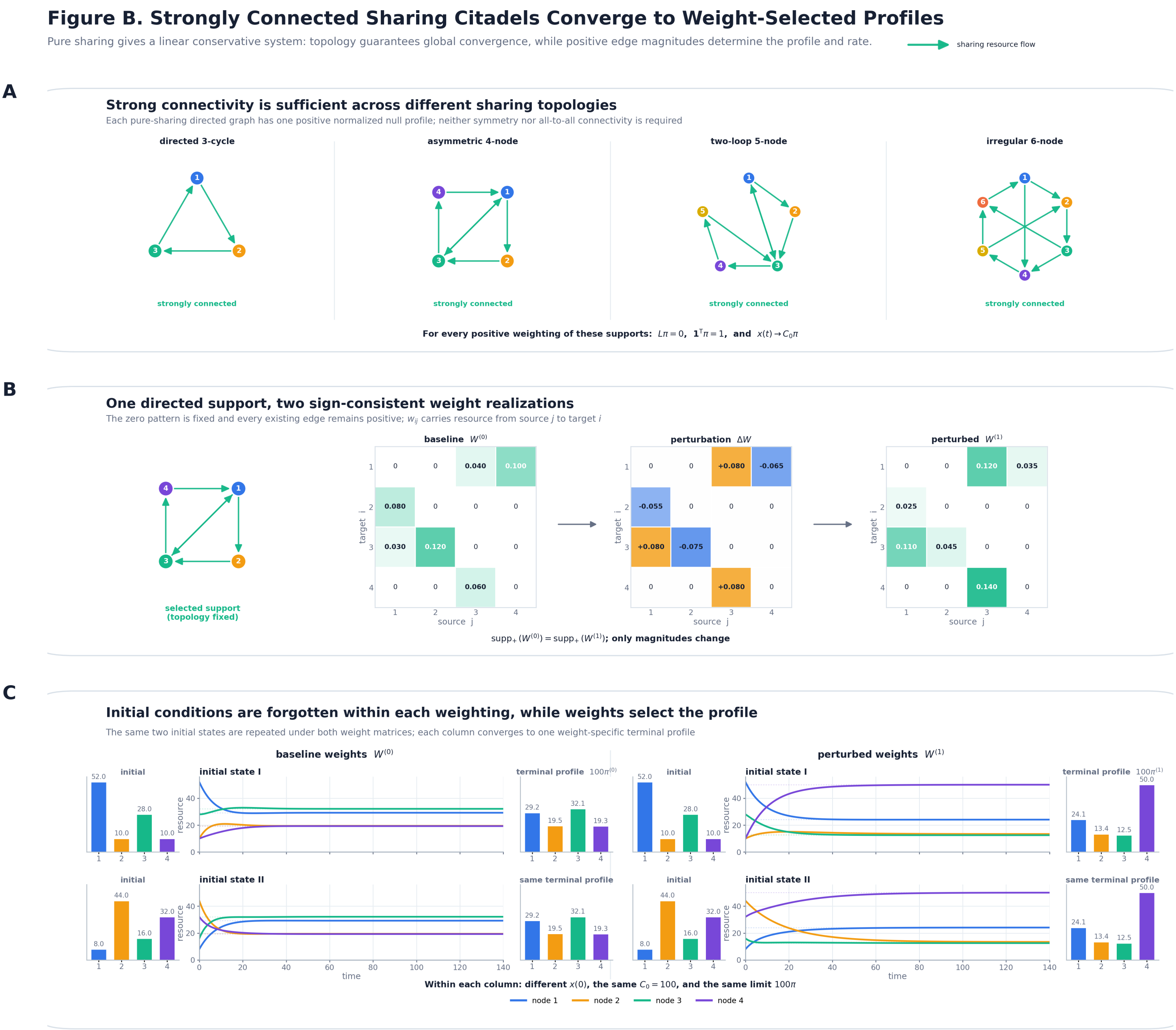

Fig. S2 Strongly connected sharing citadels converge to weight-selected profiles. (A) Four directed pure-sharing supports illustrate that neither symmetry nor all-to-all connectivity is required; strong connectivity is the shared topological condition. (B) A selected four-node support is assigned two positive weight matrices. The zero pattern and edge signs remain fixed, while the displayed perturbation changes only edge magnitudes. (C) The same two resource totals and microscopic initial states are simulated under both weight matrices. Within each column, distinct initial allocations converge to the same terminal profile. Across columns, changing the positive weights changes the profile and convergence rate without changing the existence or uniqueness of the point attractor.

Fig. C1 Three-node circulation: spectrum and restart architectures. (A) The exact conjugate eigenvalue pair separates damped, neutral, and growing rotational regimes; the nonnegative boundary converts the growing signed continuation into bounded switching. (B) Pure cyclic plundering rotates in the positive interior but reaches a one-node lock because it contains no restart path. (C1–C3) Three conservative restart architectures are compared: a same-direction sharing ring, a central neutralizer sharing with all three ports, and three internal citadel reserves. For direct comparison, all three use the same baseline magnitudes, $p = 0.100$ and $s = 0.020$. Each row shows the topology, initial state, resource trajectories, and late-time periodic orbit.

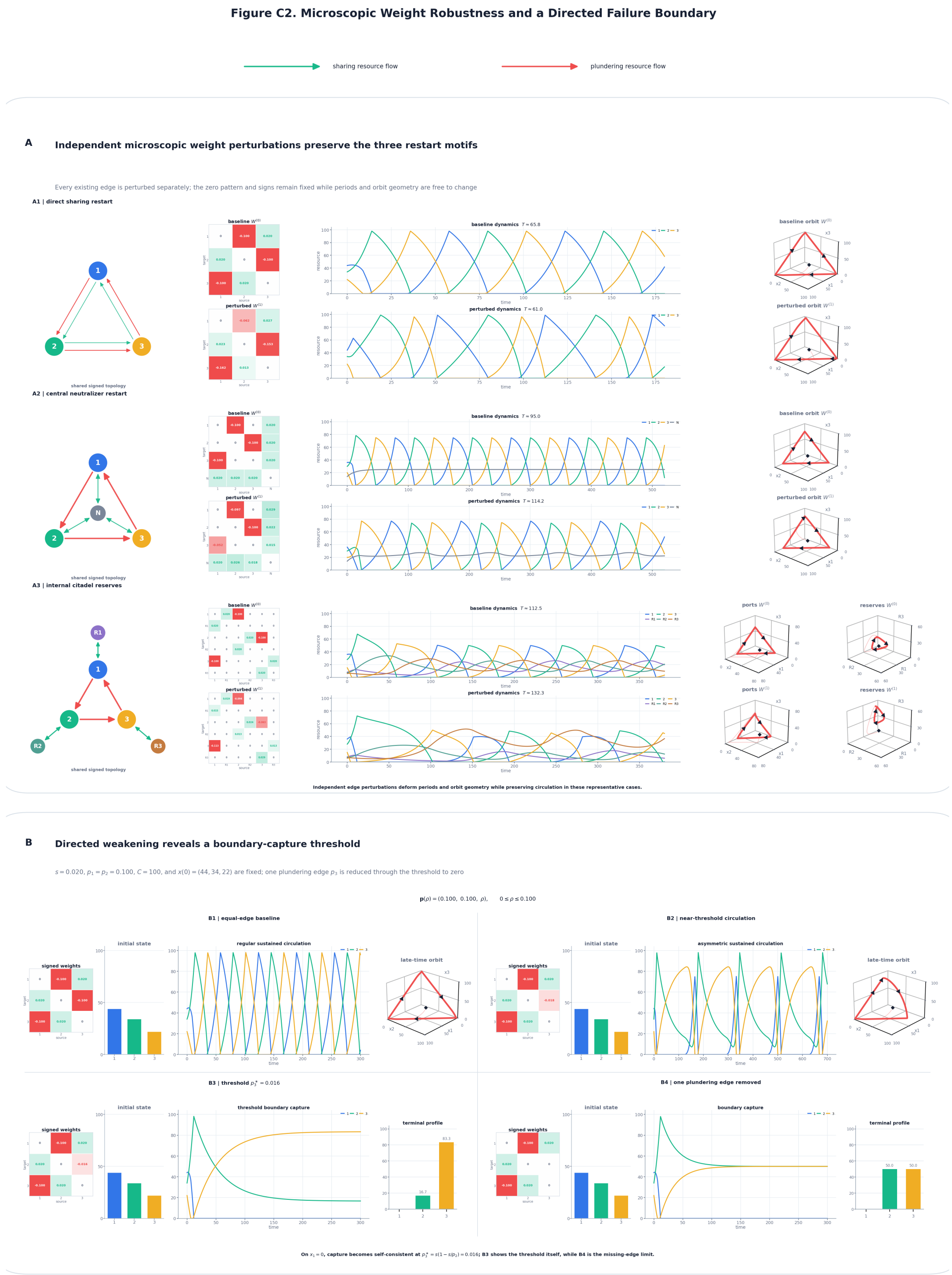

Fig. C2 Microscopic weight robustness and a directed failure boundary. (A1–A3) The direct sharing restart, central neutralizer restart, and internal citadel reserves are each represented by one signed topology spanning two experiment rows. The first row gives the baseline matrix, resource dynamics, and periodic orbit; the second gives an independently perturbed matrix and the corresponding dynamics from the same initial state. Every existing edge magnitude is perturbed separately while the zero pattern and signs remain fixed. For the internal-reserve architecture, both rows place the three-reserve orbit beside the port orbit. Periods, waveform asymmetry, and orbit geometry change, but all three systems retain sustained circulation. (B1–B4) For the direct-sharing double ring, $s = 0.020$, $p_1 = p_2 = 0.100$, $C = 100$, and the initial state are fixed while the third plundering magnitude p_3 is reduced from 0.100 to 0. Each case presents its signed weight matrix, initial bar chart, resource dynamics, and late-time attractor representation. B1 gives the equal-edge cycle and B2 remains periodic close to the capture threshold. B3 is the threshold itself, $p_3^* = s(1 - s/p_2) = 0.016$, and reaches the boundary profile $(0, 16.7, 83.3)$. B4 removes the third plundering edge and reaches $(0, 50, 50)$.

Fig. SC3 Attractor organizations beyond three-node circulation. (A) The same co-directed sharing/plundering ring is shown for three, four, five, and six nodes. All rows use $s = 0.020$, $p = 0.100$, and $C = 100$. (B) The dynamical repertoire becomes richer as ring size increases: beyond the three-node travelling wave, four nodes support a travelling wave and alternating fixed supports; five nodes support single- and mixed-wave circulation; and six nodes support single wave, double wave, and alternating fixed supports. Dynamic rows pair initial bars and resource trajectories with a late node-1-peak Poincare bar; fixed-support rows instead show their terminal profiles. The displayed alternating supports are $S_4 = \{1, 3\}$ and $S_6 = \{1, 3, 5\}$; their one-node cyclic shifts, $\{2, 4\}$ and $\{2, 4, 6\}$, are symmetry-equivalent alternatives.

Fig. D1 Far-plundering rings preserve their support geometry across node counts and weightings. (A) Six-, seven-, and eight-node systems use the same rule: nearest neighbors are unlinked and every non-neighbor pair mutually plunders. (B) The complete fixed-total adjacent-support sets are shown as sparse PCA point clouds. Pure-node states use fixed node colors, while mixed adjacent states interpolate between the two endpoint colors. These point clouds represent theoretical support complexes, not simulated trajectories. (C) For the six-node topology, a baseline matrix $W^{(0)}$, a perturbation ΔW, and the resulting matrix $W^{(1)}$ make explicit that only negative magnitudes change; the zero pattern and negative-edge support are preserved. (D) The same four initial states are simulated under $W^{(0)}$ and $W^{(1)}$, with initial bars, resource trajectories, and terminal bars shown for every run. The selected face and transient may change, but every terminal support remains an adjacent pair or a singleton boundary state.

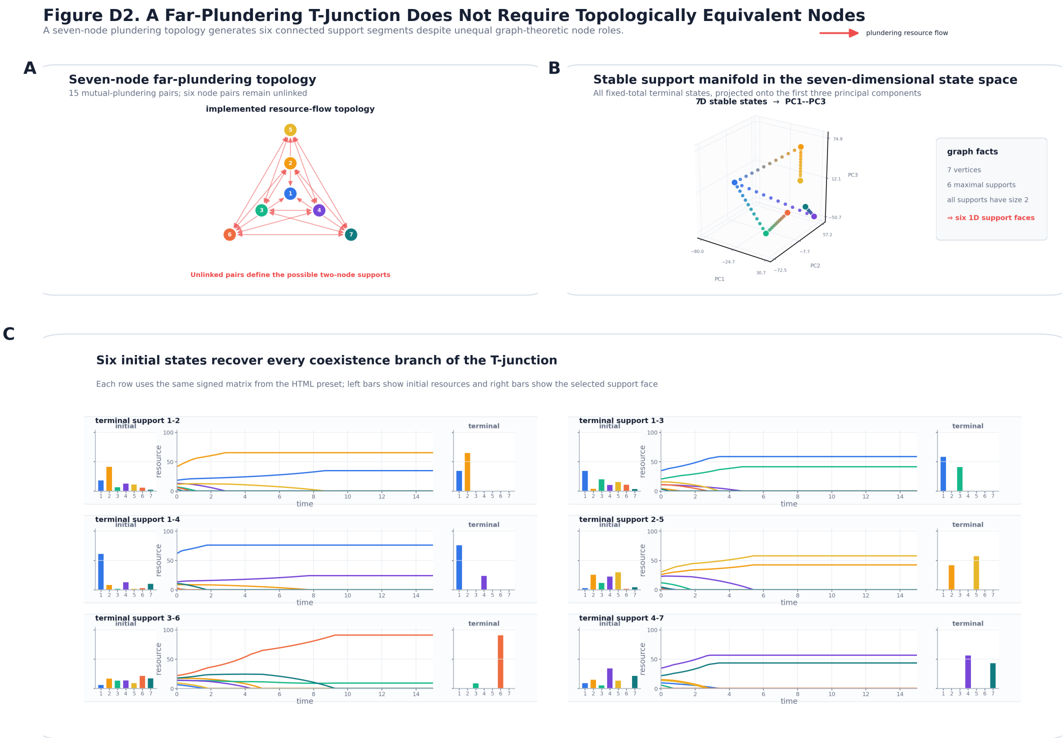

Fig. D2 A far-plundering T-junction does not require topologically equivalent nodes. (A) The actual seven-node resource-flow topology contains 15 mutual-plundering pairs and six unlinked pairs. (B) The complete stable terminal-state manifold lies in the seven-dimensional fixed-total state space; it is projected here onto its first three principal components so that all three arms remain distinct. Pure-node endpoints retain their node colors, and mixed states interpolate between endpoint colors with sparse sampling. (C) Six initial states use the same signed matrix and recover all six terminal support branches. The construction requires neither vertex transitivity, equal node degree, nor degree-dependent weight compensation.

Fig. E1 Internal sharing controls the attractor portrait of sparse citadel competition. The same two-pair sparse plundering interface is evaluated under the same four initial conditions. **A,** without internal sharing, the two WTA pairs select independently and yield four outcomes. **B,** strong sharing within X and Y produces only the two pure citadel winners. **C,** weak positive sharing preserves the pure X and pure Y winners but also leaves two mixed outcomes. Each comparison shows node trajectories and terminal profiles.

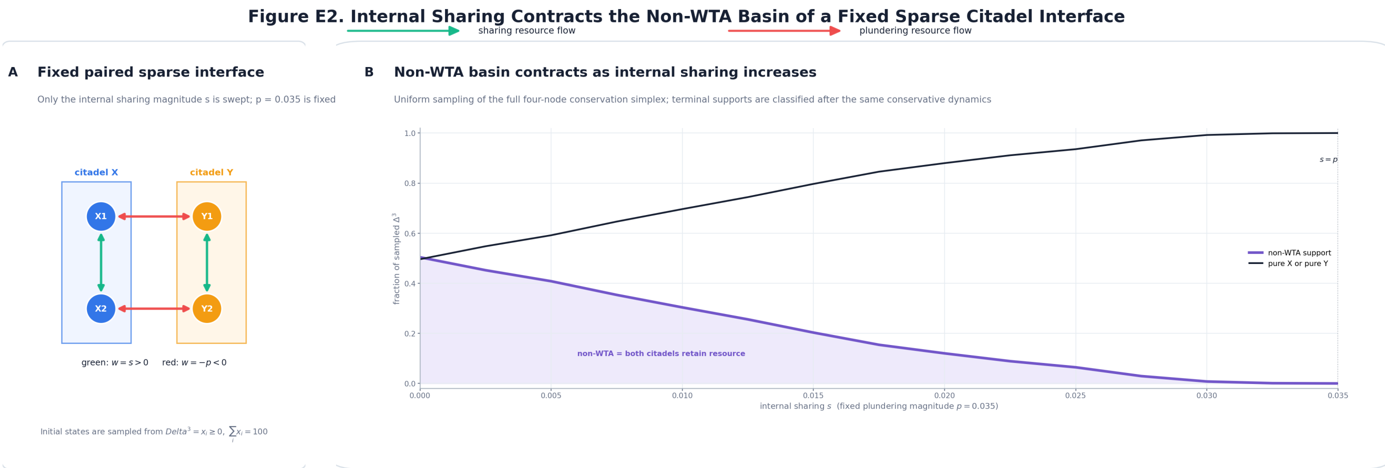

Fig. E2 Internal sharing contracts the non-WTA basin of a fixed sparse citadel interface. A, the paired sparse interface is held fixed: only the positive internal sharing weight s is swept, with plundering magnitude $p = 0.035$. **B,** uniformly sampled initial states in the full four-node conservation simplex are classified by terminal support; the non-WTA basin shrinks as s increases.

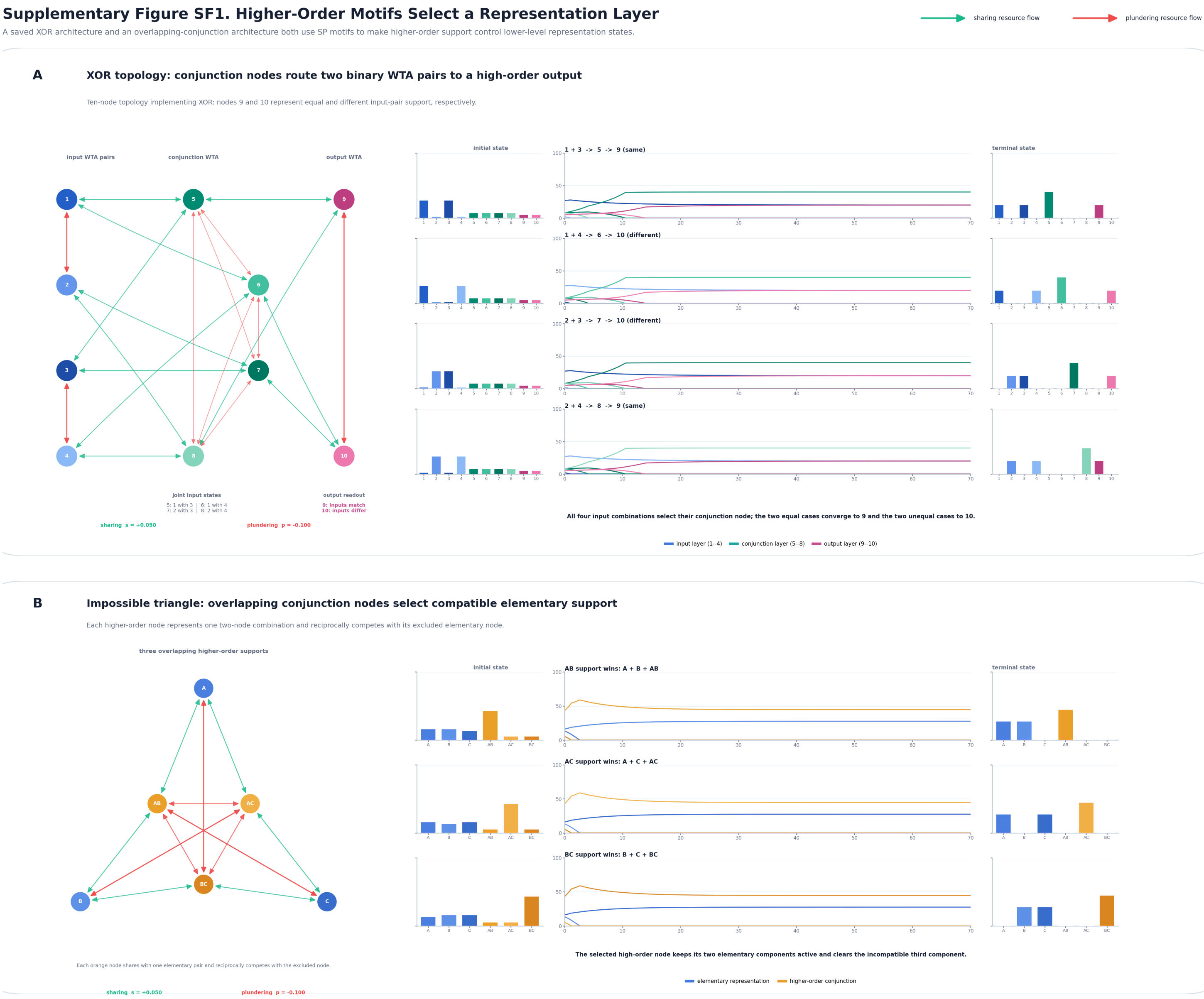

Fig. SF1 Higher-order motifs select a representation layer. A, a ten-node topology implementing the XOR relation. Two reciprocal-plundering input pairs select one of four mutually competing conjunction nodes; the output pair then selects the equal/XNOR class (node 9) or the different/XOR class (node 10). Initial bars, node trajectories, and terminal bars show all four input combinations. **B,** the impossible-triangle topology. Each higher-order conjunction node shares with a distinct elementary pair and reciprocally plunders the excluded elementary node; three initial conditions select AB, AC, or BC, together with its compatible elementary support. Green arrows indicate sharing resource flow; red arrows indicate plundering resource flow.